Experimental Investigation of a High Head Model Francis Turbine During Steady-State Operation at Off-Design Conditions

Experimental Investigation of a High Head Model Francis Turbine During Steady-State Operation at Off-Design Conditions

Carl Bergan[1], Rahul Goyal[2,3], Michel J Cervantes[1,3] and Ole G Dahlhaug[1]

[1] Department of Energy and Process Engineering, Waterpower Laboratory, Norwegian University of Science and Technology, Trondheim, Norway
[2] Department of Mechanical and Industrial Engineering department, Indian Institute of Technology, Roorkee 247667
[3] Department of Engineering Science and Mathematics, Luleå University of Technology, Luleå, Sweden

E-mail: carl.w.bergan@ntnu.no

Abstract. Francis-99 is a set of workshops aiming to determine the state of the art of high head Francis turbine simulations (flow and structure) under steady and transient operating conditions as well as promote their development and knowledge dissemination openly. The first workshop (Trondheim, 2014) focused on steady state conditions. Some concerns were raised regarding uncertainty in the measurements, mainly that there was no clear vortex rope at the Part Load (PL) condition, and that the flow exhibited relatively large asymmetry. The present paper addresses these concerns in order to ensure the quality of the data presented in further workshops.

To answer some of these questions, a new set of measurements were performed on the Francis-99 model at Waterpower Laboratory at the Norwegian University of Science and Technology (NTNU). In addition to PL, two other operating conditions were considered, for further use in transient measurements, Best Efficiency (BEP) and High Load (HL). The experiments were carried out at a head of 12 m, with a runner rotational speed of 333 revolutions per minute (rpm). The guide vane opening angle were 6.72°, 9.84° and 12.43° for PL, BEP and HL, respectively. The part load condition has been changed from the first workshop, to ensure a fully developed Rotating Vortex Rope (RVR). The velocity and pressure measurements were carried out in the draft tube cone using 2D PIV and six pressure sensors, respectively. The new PL condition shows a fully developed rotating vortex rope (RVR) in both the frequency analysis and in the phase resolved data. In addition, the measurements confirm an asymmetric flow leaving the runner, as was a concern in the first Francis-99 workshop. This asymmetry was detected at both design and off-design conditions, with a stronger effect during off design.

1. Introduction

Hydropower, being a regulated renewable energy source, is put under increasing demand to ensure a stable supply of energy. Large quantities of intermittent power sources (sun, wind, ocean wave etc.) calls for a larger amount of regulated power, while the environment calls for more renewable energy. This drives the turbines to be operated outside of their design range [1]. This operation leads to undesirable flow phenomena, which can be difficult to predict.

Phenomena such as power swings, caused by low-frequency pressure pulsations, vibration which leads to shorter lifetime for the runner, flow recirculation which lowers the runner's hydraulic efficiency. These phenomena can be difficult to predict at the design stage, and it is desirable to understand the cause and full consequences of these issues in order to mitigate them. For this, better tools in CFD are required. In performing CFD, it can be difficult to know if the results are indeed correct, particularly at part load operation, where turbulent phenomena become quite dominating [2]. While providing ample results to analyse further, CFD still lacks validation in hydropower. Francis 99 is a workshop aiming at providing the validation needed to see if the CFD provides the correct results. During the first workshop, many of the participants were able to reproduce measured phenomena with their simulations. However, there were some phenomena which the participants were unable to capture with CFD, which require experimental revaluation. Additionally, several concerns have been raised about the experimental work submitted to the previous Francis-99 workshop, so the goal of this paper is to assess those concerns, while providing supplementary experimental data.

2. Materials and Methods

The measurements were performed in the Waterpower Laboratory at NTNU, on the Francis-99 runner. The Francis-99 runner is a 1:5.1 scaled model of a prototype in a Norwegian power plant called Tokke. The turbine consists of a spiral casing with 14 stay vanes, 28 guide vanes, and a runner with 15 full-length blades and 15 splitter blades, for a total of 30 runner blades. The measurements were performed at three operating points: Part Load (PL), the Best Efficiency Point (BEP) and High Load (HL). The specifics of these operating points are given in table 1

Table 1: Description of the operating points

Operating Point	Head H [m]	Flow Rate Q [m^3/s]	Specific speed n_{ED} [-]	Specific flow Q_{ED} [-]	Hydraulic efficiency η [-]
PL	11.87	0.140	0.179	0.106	0.901
BEP	11.94	0.200	0.179	0.152	0.924
HL	11.88	0.242	0.179	0.184	0.917

The operating conditions are inspired by the operating conditions presented in Francis99(I) [3], but with some changes. Since the goal is to perform realistic transient measurements, the operating points have been changed to have the same RPM for all operating conditions. Additionally, the part load operating condition has been changed in order to capture a more fully developed Rotating Vortex Rope. In order to maintain some similarity to the operating points presented in Francis 99 (I), the value for n_{ED} was maintained constant for the BEP condition. The measurements were performed in an open loop configuration, shown in figure 1

The measurements with PIV is based on the analysis of two successive images of the target area seeded with micro-sized particles that follow the flow and that are illuminated with a laser sheet provided by double-pulsed laser [4]. The PIV measurements have been performed in the draft tube with a TSI 2-D system. Draft tube are made of transparent Plexiglas's to allow the laser sheet and to capture the successive images in the flow domain. The pulsed light sheet with a thickness of approximately 3 mm, is generated by two Nd:YAG PIV laser (Maximum frequency=50 Hz) with dual cavity performing 100 mJ by pulse. The wavelength is 532 nm.

The lightning field is visualized by a low noise digital CCD camera (VC-4MC-M180) of 2400x2400 pixel resolution, with a succession of paired images at 300 µs to 400 µs. The camera

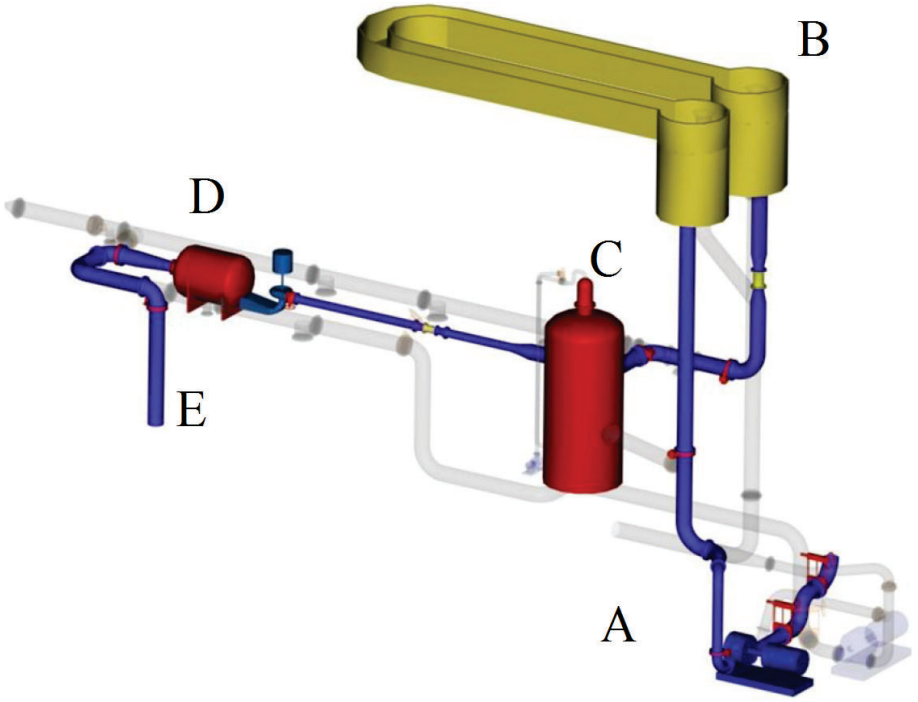

Figure 1: Open loop test rig. The water is pumped from the lower reservoir (A) to the upper reservoir (B). The channel between the two overhead tanks in (B) ensure that the pump and turbine are hydraulically separated. The overhead tanks are fitted with overflow pipes, to ensure a constant upstream water level. The water then enters the pressure tank (C), which will act as an air cushion chamber. The water then passes through an electromagnetic flowmeter before entering the turbine. After leaving the turbine, the water enters the draft tube tank, where an overflow wall maintains the downstream water level. Finally, the water leaves the downstream tank, returning to the lower reservoir (E)

resolution is 2032 x 2048 pixels for a 276.0 x 278.0 mm^2 spatial domain.

TSI seeding particles with a density of 1.016 g/cm^3, refractive index 1.52 and mean diameter of 55 µm were used for the measurements. Since the camera is capable to capture the image in pixel displacement, a magnification factor (α) or mathematical constant is required to covert the pixel imaging chip to a physical distance in real space. Due to the conical shape of the draft tube and coupled different angle of refraction a correction in optical distortion is required. To minimize the optical distortion, an index matching box (refractive index 1.52) made of glass filled with water, was used during the calibrations and measurements to decreases the light aberration during the PIV measurements. The ex-situ calibration was performed in the draft tube due to practical limitations associated with the in-situ calibrations. A specially designed 2-D target plate with the dots having the diameter of 2 mm and space between the dots is 20 mm was placed inside the draft tube to compensate the light aberration as shown in Figure 2.

The aberration will still exists close to the areas of high curvature i.e., close to the draft tube wall. As seen in the figure 2 (left) there is distance between the draft tube wall and the first calibration point. Hence, the calibration results are extrapolated close to the wall. Moreover, the picture is warped significantly close to the wall but unaffected along the cone centerline. Thus, the calibration matrix calculated may be subject to the some uncertainties close to the

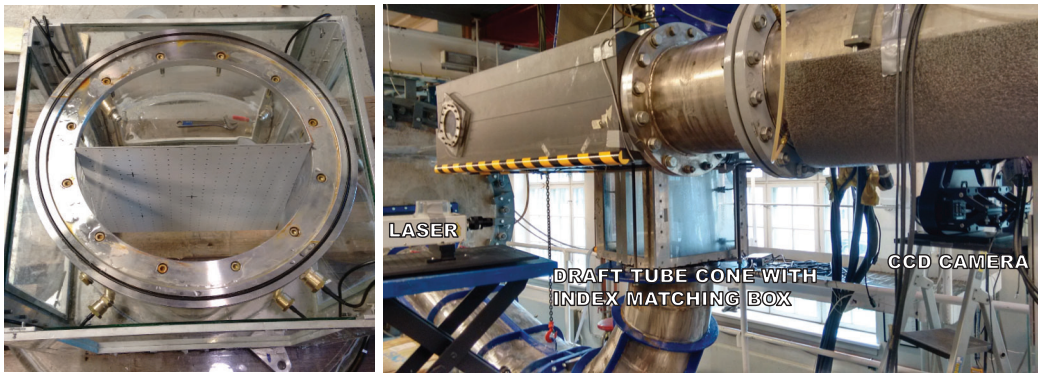

Figure 2: Calibration setup

wall. Therefore, calibration and measurement plane was selected few mm away from the draft tube walls to avoid the aberration as shown in Figure 3. The target plate was placed in the respective measurement plane and photographed by the camera of the PIV system. During the calibration the camera is exactly at the same position as later in the measurements. The images were recorded at a rate of 40 Hz. 2400 paired images for 60 s were captured at the measurement section. Number of images were selected on the basis of required convergence images for steady-state operation. So that the complete convergence in steady-state data before and after the transition in transient operation can be achieved.

The measurement section, along with the pressure sensor placement is shown in Figure 3.

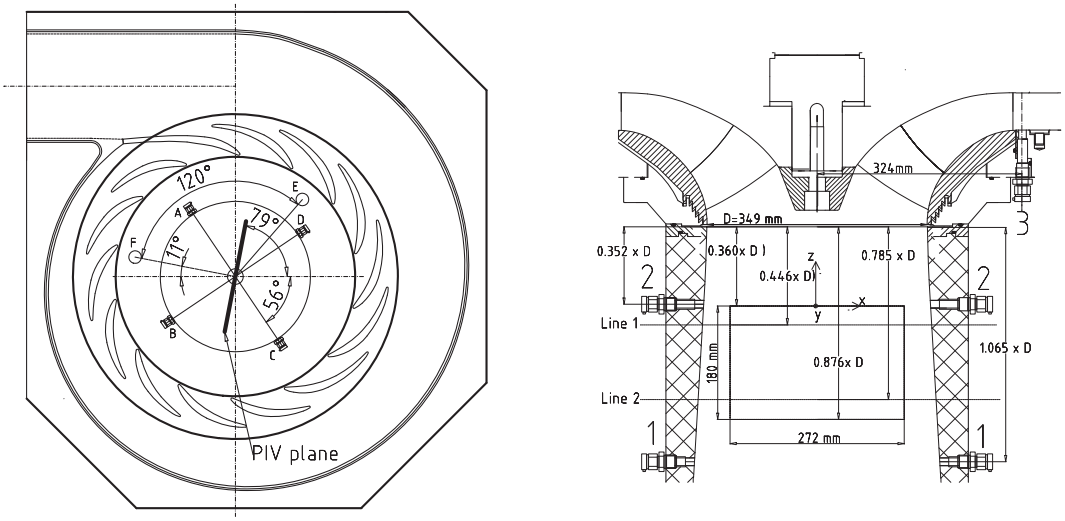

Figure 3: Sensor placement as seen from top (left) and from the side (right). The sensors corresponding to the numbers are shown in table 2

The position of the individual pressure sensors is shown in Table 2.

The pressure measurements were recorded using a National Instruments (NI) Compact Reconfigurable Input/Output (cRIO) Model 9074 with a 24 bit analog to digital converter (ADC). The data was recorded at 5 kS/s with a separate ADC for each channel. The regular

Table 2: Position of the draft tube pressure taps

Sensor	Placement	Type
DT1	1A	Kistler
DT2	1B	Kistler
DT3	1C	Kistler
DT4	1D	Kistler
DT5	2B	Kistler
DT6	2D	Kistler
VL1	3E	Kulite
VL2	3F	Kulite

test rig instrumentation yields values for flow, head, generator torque and runner frequency. In addition to the base instrumentation of the test rig, six pressure taps were mounted on the draft tube cone, and two in the vaneless space as shown in Figure 3.

3. Results and Discussion

As mentioned before, the PL operating condition used in the first Francis-99 workshop was infeasible to perform simulations on. The participants called for a different PL operating point, with a more clearly defined vortex rope.

Figure 4 shows the Fast Fourier Transform (FFT) results from the draft tube pressure sensors at PL operation.

A new operating condition was therefore chosen for part load, with the restriction of having the same rotational speed as the BEP and HL operating conditions. The amplitude of the RVR frequency was used as a guide for choosing a suitable part load operating point. The results show a strong rotating vortex rope at 1.633 Hz (corresponding to $0.294 f_n$), with both the 2nd and 3rd harmonic present. In addition, some noticeable oscillations can be observed at 15.8 Hz and 41.8 Hz, for all the sensors. Assuming the speed of sound in the pipe system to be 1100 m/s, the estimated frequency for a standing wave is approximately 15.6 Hz between the runner and the pressure tank, and 39.3 Hz between the runner and the draft tube tank. Due to the uncertainty in estimating the speed of sound in the pipe system, it is reasonable to assume that the signals at 15.8 Hz and 41.8 Hz are standing waves. Decomposing the pressure signals from the draft tube cone into its rotating and plunging components yields the results shown in Figure 5

Since the 15.8 Hz and 41.8 Hz frequencies are present only in the synchronous portion of the signal, they are considered to be standing waves.

3.1. Phase resolved vortex rope

The data can be reduced into three components using Reynolds triple decomposition: the time-averaged velocity, $\overline{\phi}(x)$; oscillatory part, $\widetilde{\phi}(x,t)$; and the random fluctuations, $\phi'(x,t)$. This decomposition is shown in Equation 1 [5]

$$\phi(x,t) = \langle \phi(x,t) \rangle + \phi'(x,t) = \overline{\phi}(x) + \widetilde{\phi}(x,t) + \phi'(x,t) \tag{1}$$

By phase resolving the signal for a chosen frequency, and placing the data in phase-averaged bins, cyclic phenomena which may even be of higher frequency than the measurement's Nyquist frequency become evident. This is shown in Figure 6, where the PIV measurement during Part load is sampled at one point in the measurement section, and phase resolved with the runner

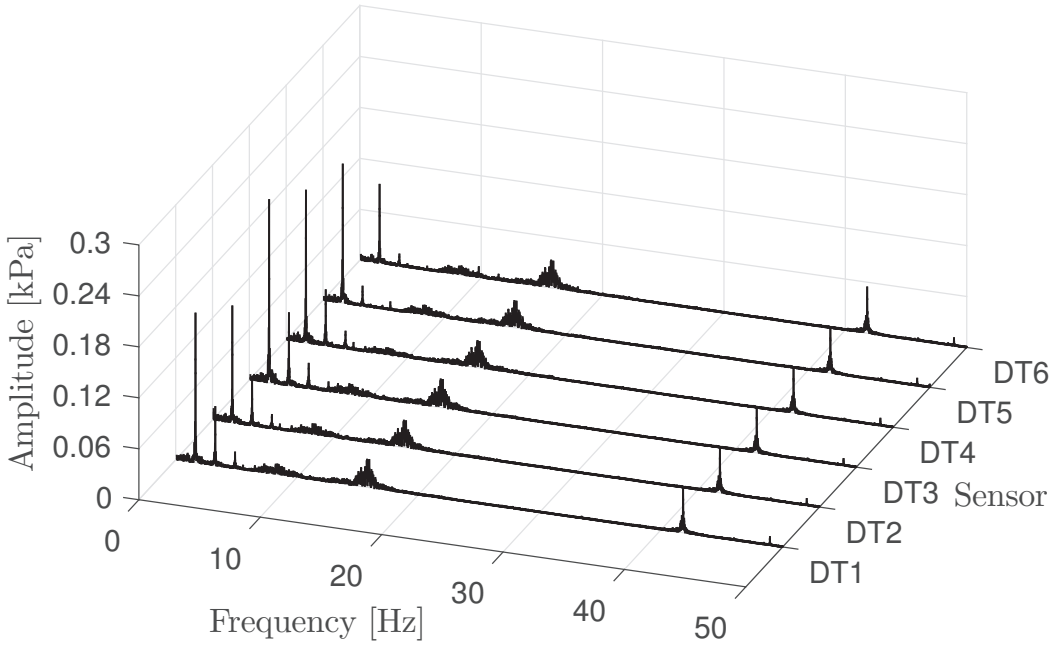

Figure 4: Waterfall diagram of the PL operation. Note the small peak at 16 Hz, and the sharper peak at 42 Hz. These are thought to be standing waves in the inlet and outlet pipe, respectively.

frequency. Applying this method for multiple points along the radius yields the figure shown in Figure 6, right.

Phase resolving the data with respect to the RVR frequency clearly shows that there is indeed a fully developed rotating vortex rope in the flow, shown in Figure 7.

The new part load condition can therefore be used for further measurements and simulations on the Francis 99 workshops.

3.2. Velocity profiles

The axial velocity profiles for BEP and PL are shown in Figure 8. Both operating points show signs of asymmetry, which can also be seen in the radial velocity profile. This point was raised at the first Francis-99 workshop. Multiple repetitions were performed for each operating point in order to firmly establish the measurement uncertainty.

Both the axial and the radial velocities show signs of asymmetry. This is most likely due to the gyroscopic effect introduced by the draft tube elbow, in addition to an uneven distribution of water in the spiral casing. The measurements were performed near the middle of the draft tube cone, in order to better capture the asymmetric flow.

The asymmetry at BEP is shown in Figure 9. The difference in mean axial velocity over the centerline of the draft tube cone varies with operating point and with vertical position in the draft tube cone. For BEP, the difference in axial velocity is 3.7% in the upper line, and 10.7% in the lower line. For PL, the difference is 64.2% in the upper line, and 67.1% in the lower line. The relative difference in PL appears to be very large, but this is due to the bulk velocity being quite low at this operating condition. Nevertheless, it shows that the flow is

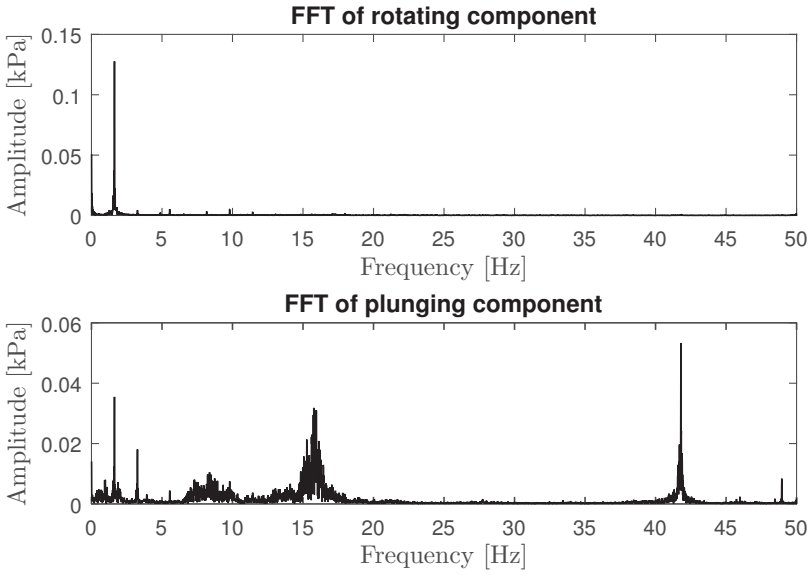

Figure 5: FFT analysis of the rotating and plunging components at the PL operating condition

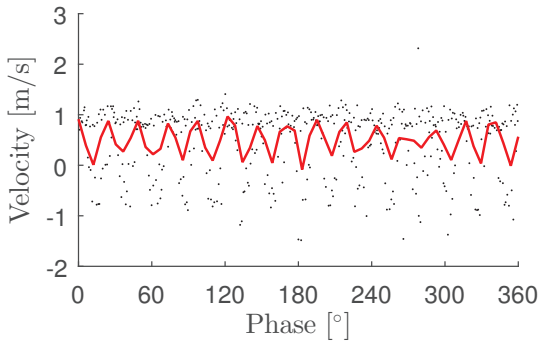

(a) Phase resolved velocity for one point in space r^* =0.51. The bin size is 6 degrees, and the number of samples per bin is approximately 100. The red line indicates the mean value within each phase bin, while the black dots are all the measured velocities.

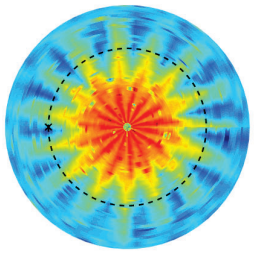

(b) Phase resolve performed for the whole measured cross section. The location of the point investigated in the left figure is indicated with the black marker.

Figure 6: Velocity measurements phase resolved with respect to the runner frequency, sampled at PL operation. The velocity is sampled at 0.59xD downstream the draft tube inlet. The velocity component shown in this figure is the axial velocity.

becoming increasingly asymmetric in the flow direction. The asymmetry is large, and increasing in the stream direction for all operating conditions. This indicates that the asymmetric flow is indeed originating from the gyroscopic effect of the draft tube elbow. In addition to exhibiting significantly asymmetric flow, the PL operating condition shows signs of a recirculation zone with negative axial velocity. In the PL velocity profile, shown in figure 8, the axial velocity is nearly zero close to the draft tube center, even though this is some distance downstream the draft tube inlet. In addition to that, the RVR exhibits a large internal region of negative

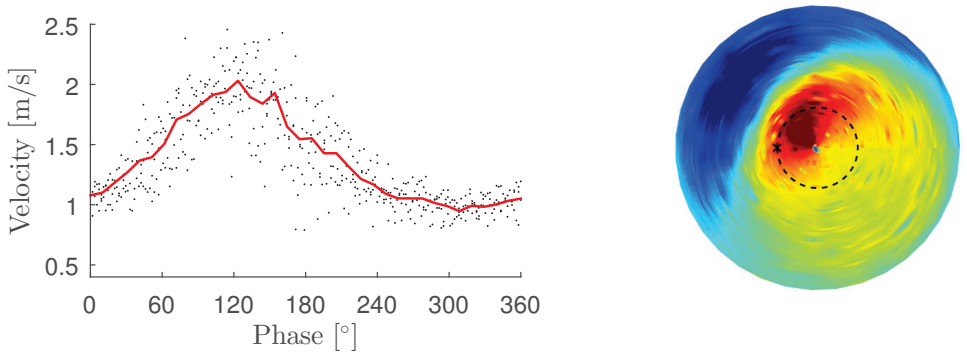

(a) Phase resolved velocity for one point in space r^* =0.22. The bin size is 10 degrees, and the number of samples per bin is approximately 100. The red line indicates the mean value within each phase bin, while the black dots are all the measured velocities.

(b) Phase resolve performed for the whole measured cross section. The location of the point investigated in the left figure is indicated with the black marker.

Figure 7: Velocity measurements phase resolved with respect to the RVR frequency, sampled at PL operation. The velocity is sampled at 0.59xD downstream the draft tube inlet. The velocity component shown in this figure is the axial velocity.

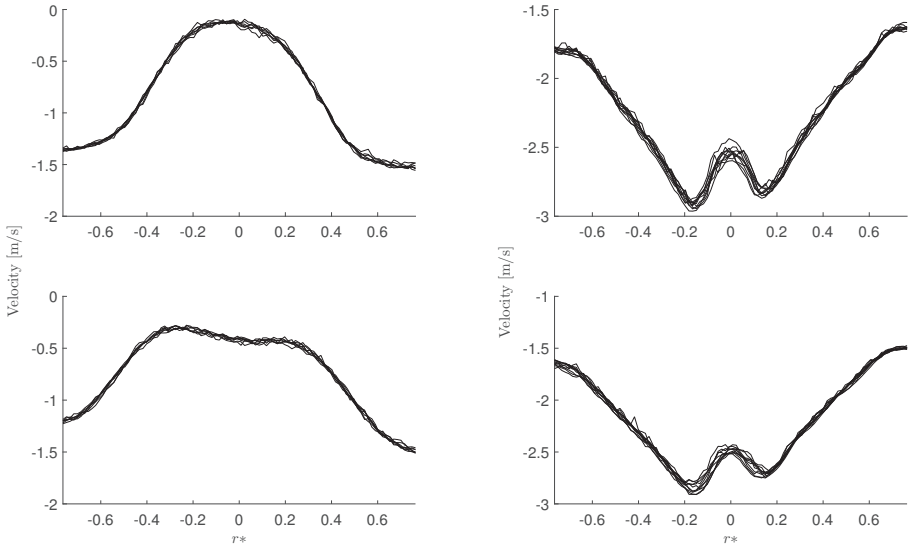

(a) PL axial velocity

(b) BEP axial velocity

Figure 8: Axial velocity profiles. The upper graphs depict the velocity at Line 1, while the lower graphs depict the velocity at Line 2, as shown in Figure 3. r^* is the dimensionless radius, obtained by reducing the radius at the measurement location with the radius at the draft tube inlet. Note that the velocity is not symmetric about the centerline, and that this asymmetry gets relatively larger for the lower graphs.

axial velocity, indication a large internal recirculation in the RVR. These effects combined are significant in reducing runner efficiency at PL operation.

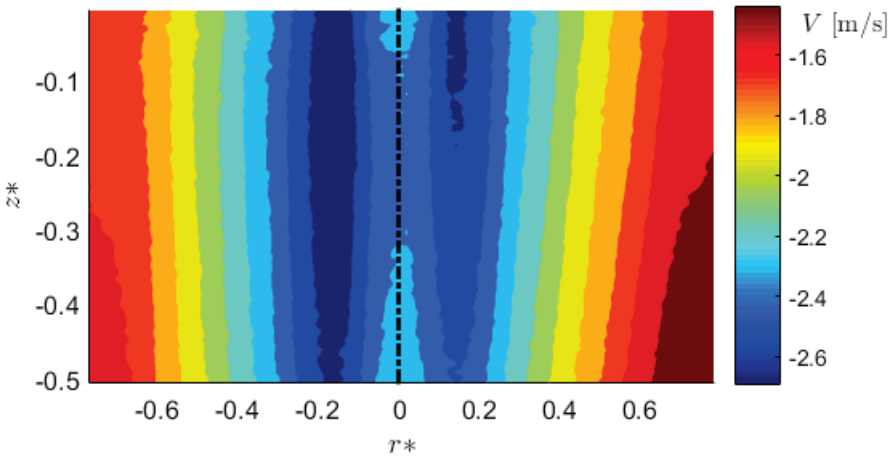

Figure 9: BEP asymmetry. The dashed line indicates the centerline of the draft tube cone. In this measurement, the mean difference in axial velocity over the centerline is approx. 7.6%, with a higher axial velocity on the left side of the centerline. r^* is the dimensionless radius, obtained by reducing the radius at the measurement location with the radius at the draft tube inlet.

4. Conclusions

The new part load condition exhibits a clear vortex rope with internal recirculation, and is therefore considered to be appropriate for further simulation during the coming Francis 99 workshops. The Vortex rope can be seen in the velocity data through both frequency analysis and phase resolving. Additionally, the runner blade wakes are clearly visible in the phase resolved results, but the splitter blades are not evident in the velocity data. This indicates a good mixing of the channel flows in the runner downstream the splitter blades. The results show that the part load condition has a strongly developed rotating vortex rope, consisting of both rotating and plunging components. The FFT also reveals a clear standing wave in the results, something that could be captured with CFD, if desired. The flow exhibits a relatively high degree of asymmetry, yielding a difference in axial flow of 10.7% for BEP and 67.1% for PL. The asymmetry is increasing in the flow direction, becoming more significant near the draft tube elbow.

References

[1] C. Trivedi, B. Gandhi, and C. J. Michel. "Effect of transients on Francis turbine runner life: a review". en. In: *Journal of Hydraulic Research* 51.2 (Apr. 2013), pp. 121–132.

[2] Z. Yaping et al. "Performance study for Francis-99 by using different turbulence models". In: *Journal of Physics: Conference Series* 579 (Jan. 2015), p. 012012.

[3] C. Bergan et al. "Preliminary Measurements of the Radial Velocity in the Francis-99 Draft Tube Cone". In: *Journal of Physics: Conference Series* 579 (Jan. 2015), p. 012014.

[4] M. Raffel et al. *Particle Image Velocimetry A Practical Guide*. English. Berlin, Heidelberg: Springer-Verlag Berlin Heidelberg, 2007.

[5] K. Amiri. "An experimental investigation of flow in a Kaplan runner steady-state and transient". Licentiate. LTU, 2014.